IEEE Access
Multidisciplinary | Rapid Review | Open Access Journal

Received 17 March 2026, accepted 13 April 2026, date of publication 23 April 2026, date of current version 19 May 2026.

Digital Object Identifier 10.1109/ACCESS.2026.3686971

RESEARCH ARTICLE

A Fine-Tuned Fuzzy-Optimized UNet++ for Retinal Vessel Segmentation

KUMAR JANARDAN PATRA[1], JIBITESH MISHRA[1], SANJIT KUMAR DASH[1], DIPAK KUMAR NIDHI[2], SUDHIR KUMAR MOHAPATRA[2], JUKKA HEIKKONEN[2], AND RAJEEV KANTH[3], (Senior Member, IEEE)

[1]Odisha University of Technology and Research, Bhubaneswar, Odisha 751029, India
[2]University of Turku, 20014 Turku, Finland
[3]Savonia University of Applied Sciences, 70210 Kuopio, Finland

Corresponding author: Sudhir Kumar Mohapatra (skmoha@utu.in)

ABSTRACT The human eye is a vital organ responsible for vision, and the health of the retina is crucial for preserving sight. Retinal vessel segmentation plays a key role in the early detection of ophthalmic diseases such as diabetic retinopathy, glaucoma, and hypertension, where vascular abnormalities indicate disease progression. This study introduces a novel hybrid framework that enhances vessel segmentation performance using Fuzzy-Optimized UNet++ architecture, demonstrating a 2% improvement over the baseline UNet++ (95.3% accuracy). The proposed method is trained and validated on five benchmark datasets DRIVE, HRF, IOSTAR, ARIA, and CHASE_DB1, offering diversity in image resolution, pathology, and vessel morphology to evaluate cross-dataset generalization potential. To address limitations such as class imbalance, noise sensitivity, and poor micro-vessel continuity, we incorporate fuzzy logic for enhanced boundary refinement and Harris Hawks Optimization (HHO) for robust parameter tuning and convergence acceleration. Additionally, a synthetic vessel generation module, VesselGAN, is used to expand dataset diversity, achieving an SSIM score of 0.89 while preserving anatomical accuracy. Comprehensive evaluation is performed using 10-fold cross-validation and external testing on five independent datasets RETA, IDRiD, IOSTAR (external), Kaggle, and clinical-grade images. The integrated approach achieves improved performance across key metrics, including Dice Coefficient, IoU, SSIM, and F1-score, especially under noisy, low-contrast, and ultra-thin vessel conditions. This research presents a unified, end-to-end system that advances the state-of-the-art in retinal vessel segmentation. Its superior accuracy, resilience to data variability indicates robustness across unseen clinical domains and suggest suitability for real-world deployment in ophthalmic diagnostic systems.

INDEX TERMS Biomedical imaging, HHO, fuzzy logic, image segmentation, U-Net++, vessel GAN, retinal vessel.

I. INTRODUCTION

The retina, a thin tissue layer at the back of the eye, is essential for detecting light and transmitting visual information to the brain. Its blood vessels ensure proper nourishment and oxygenation of the retina. Any disruption or abnormality in these vessels can cause severe vision problems or even blindness. Retinal vessel segmentation, which involves extracting the vascular structures from retinal images, plays a crucial role in diagnosing eye conditions like diabetic retinopathy, age-related macular degeneration, glaucoma, and hypertensive retinopathy [1]. These diseases alter the retinal vasculature and, if not treated promptly, can lead to permanent vision loss. Early detection, [2] often achieved through analyzing retinal vessels, is key to managing these conditions and preventing irreversible damage. Automated retinal vessel segmentation plays a crucial role in improving diagnostic accuracy and reducing the burden of

The associate editor coordinating the review of this manuscript and approving it for publication was Mouloud Denai.

manual analysis, highlighting the need for precise and reliable algorithms. This highlights the need for advanced, precise algorithms that can accurately segment retinal vessels, ultimately enhancing diagnostic processes in ophthalmology [3].

In recent years, deep learning (DL)-based models have significantly advanced the field of medical image segmentation, particularly in retinal vessel extraction. Convolutional Neural Networks (CNNs), such as U-Net, U-Net++, ResNet, and DeepLabV3+ [4] have demonstrated promising results in detecting retinal structures. U-Net++ has emerged as a popular model due to its nested skip connections and multi-scale feature extraction, improving segmentation performance in medical imaging [5]. Despite notable advancements, current segmentation models face significant limitations that hinder clinical deployment. Despite notable advancements, existing models face limitations such as class imbalance, sensitivity to noise and image quality variations, and difficulty in accurately segmenting thin vessels. Additionally, limited validation on real clinical data restricts their practical deployment.

To tackle the limitations of conventional segmentation methods, we propose a Fine-Tuned Fuzzy-HHO UNet++ model, a novel hybrid architecture that combines fuzzy logic-based enhancement and Harris Hawks Optimization (HHO) with UNet++ for retinal vessel segmentation. The key contributions of this work include:

- Introduced a dual-stage fuzzy module for vessel edge enhancement and morphological refinement, improving detection of fine, low-contrast structures.
- Employed VesselGAN for synthetic retinal image generation, effectively increasing dataset diversity and to enhance model generalization and reduce overfitting it implemented data augmentation techniques.
- Integrated HHO-based adaptive feature selection and parameter optimization within the UNet++ framework, enabling dynamic learning beyond conventional optimization-based UNet models.
- Optimized vessel segmentation accuracy using a lightweight yet adaptive framework, enabling better convergence and class balance across vessel and background pixels.
- Validated across four diverse retinal datasets (RETA, IOSTAR, KAGGLE, IDRiD) to ensure clinical relevance, generalizability, and real-world robustness.
- Outperformed baseline UNet++-based models under low-contrast and noisy conditions in terms of Dice, IoU, SSIM, and AUC metrics.

The proposed Fuzzy-HHO UNet++ framework presents a robust and computationally efficient solution for retinal vessel segmentation. Unlike earlier fuzzy-based architectures such as Fuzzy-CNN and Fuzzy-ResUNet, which rely solely on contrast enhancement, or optimization-driven models like PSO-UNet and GA-DeepSeg that focus only on hyperparameter tuning, this method uniquely integrates fuzzy logic and metaheuristic optimization within a unified U-Net++ backbone. This dual integration enables simultaneous enhancement of vessel boundary sharpness and adaptive weight optimization, achieving superior convergence stability and vessel continuity.

The effectiveness of the proposed framework is evaluated through comprehensive experiments, including cross-validation and external dataset testing. The model demonstrates consistent and improved performance compared to the baseline UNet++, particularly in capturing fine and low-contrast vessel structures. The integration of VesselGAN contributes to enhanced data diversity, while the overall architecture maintains a balance between segmentation accuracy and computational efficiency, indicating its suitability for practical applications.

To further highlight the innovation of the proposed approach, it is important to distinguish it from existing fuzzy-based and optimization-based UNet variants. Traditional fuzzy-based models primarily focus on local contrast enhancement and rule-based boundary refinement, often lacking adaptability at the feature-learning level. On the other hand, optimization-driven approaches such as PSO-UNet and GA-based UNet models mainly concentrate on hyperparameter tuning without directly enhancing structural feature representation. In contrast, the proposed Fine-Tuned Fuzzy-HHO UNet++ integrates dual-stage fuzzy enhancement with HHO-based adaptive feature and parameter optimization within a unified architecture. This combined design enables simultaneous improvement in vessel boundary delineation and deep feature learning, which is not jointly addressed in prior methods.

The remainder of this paper is organized as follows: Section II reviews related works on retinal vessel segmentation. Section III details the proposed methodology. Section IV describes the architecture and design of Fuzzy-Optimized UNet++. Section V presents experimental results and analysis. Section VI discusses the ablation study. Finally, Section VII concludes the paper with limitation and future work.

II. LITERATURE REVIEW

Recent developments in image segmentation have significantly advanced the field through innovative methodologies, particularly in the medical domain. Several enhanced models have demonstrated improved resistance to noise, edge enhancement, and better preservation of object dimensions. For example, models like Fuzzy Moving K-Means and Adaptive Fuzzy Moving K-Means (AFMKM) [6], and the fuzzy rule-based image enhancement system [7], provide greater flexibility and robustness in image processing tasks. To handle spatial and spectral complexities in high-resolution data, the F-UNet++ framework [8] was developed for multispectral and panchromatic image fusion. This foundational advancement paved the way for more specialized models tailored to retinal disease diagnosis. In the context of retinal lesion segmentation, GAGUNet [11] integrates graph convolution networks with an attention-based UNet architecture for segmenting SD-OCT images. It significantly

improves segmentation accuracy, achieving a pixel accuracy of 0.8065 on the RETOUCH dataset. MU-Net [10] proposes a modified U-shaped network incorporating residual attention and selective kernel modules. By capturing multi-scale features and improving microvessel connectivity, MU-Net achieves a high average segmentation accuracy of 98%. Building on multi-scale feature integration, MSR U-Net [19] introduces residual blocks and bottleneck residual paths, demonstrating enhanced performance across multiple datasets. While validated by medical experts, further expansion is needed for its application to diverse clinical environments. To segment lesions like microaneurysms and hard exudates, an encoder–decoder network using channel-wise attention was proposed [12]. Tested on the IDRiD dataset, it achieved an impressive 99.94% accuracy. A transformer-based UNet model with a dual-path decoder [13] was later introduced to improve thin vessel segmentation, using a semi-supervised strategy that leverages rough skeleton annotations. Although this method reduces annotation burden and achieves strong performance, it requires better handling of annotation errors for clinical reliability. A different approach SPORG-RBVS [14] combines the Sandpiper Optimization algorithm with region-growing techniques for robust segmentation of complex vessel patterns. It showed strong generalization and accuracy on DRIVE, STARE, and CHASE_DB1, outperforming many traditional techniques in handling intricate vascular structures. To further reduce computational overhead while maintaining accuracy, Decom-UNet3+ [15] was introduced. It replaces standard convolutions with decomposed convolutions and integrates spatial attention. A hybrid approach [16] combining dynamic segmentation, Elephant Herding Optimization, and a Q-LGAN-enhanced autoencoder was developed for Diabetic Retinopathy detection. In training data diversity and fine boundary delineation, DS-AdaptNet [17] integrates a novel morphological perturbation augmentation technique (MD-PAT) and a context-aware adaptive thresholding algorithm (CA-ATO). With only 1.57M parameters and 44.08 GFLOPs, Finally, lightweight encoder–decoder architectures optimized for embedded platforms [18] demonstrated promising results across same data. Despite a significant reduction in computation and memory requirements, the model maintained competitive performance.

The reviewed models highlight significant strides in retinal image segmentation through deep learning innovations, attention mechanisms, and optimization strategies. While many achieve high accuracy and efficiency, challenges like artifact misclassification, fine vessel segmentation, and clinical deployment persist. However, most existing fuzzy-based approaches focus primarily on local contrast enhancement, and optimization-driven methods such as PSO- and GA-based UNet variants mainly target hyperparameter tuning without addressing feature adaptability. In contrast, our proposed Fine-Tuned Fuzzy-HHO UNet++ integrates fuzzy logic and metaheuristic optimization within a unified framework, enabling adaptive feature enhancement and parameter refinement simultaneously. These insights guide the development of more robust, scalable, and clinically viable solutions.

TABLE 1. Summary of existing studies with corresponding limitations and key findings.

Author's	Year	Data Used	Model	Limitation	Performance Metrics
G. B. Kande, et al. [9]	2023	DRIVE, STARE, CHASE_DB1	MSR U-Net	• Challenging on extensive and diverse preprocessed data for optimal training • Limited to retinal vessels • Random cropping may miss certain vessel patterns.	Accuracy: 0.978, AUC: 0.985, Sensitivity: 0.95, Specificity: 0.964
B. N. Kumar, et al. [10]	2023	IDRiD	DL-UNet	• level focus lacks spatial context • Sensitive to image quality • Class imbalance	Accuracy: 99.94%, Precision: 98.47%, Recall: 98.36%, Dice: 0.9998
D. Oh et al. [11]	2024	RETOUCH, Konkuk Hospital SD-OCT	GAGUNet	• Mislabeling of artifacts as lesions • Lack of noise reduction • Limited extensive annotated datasets for training robustness	Dice: 0.8306, Accuracy: 0.8065, Sensitivity: 0.8181, Specificity: 0.9995
He. X, et al. [12]	2024	Children's Hearing and Health Research Project (UK)	MU-Net	• Discontinuity in micro vessel segmentation • Limited sensitivity for tiny vessels • Needs better contrast handling	Avg Acc-0.98 Avg MCC score -0.83
Y. Zhang, et al. [13]	2024	Public fundus datasets	TSNet	• Does not handle annotation errors • Needs improved robustness for mislabeled or incomplete training data • Requires better error tolerance • Thin vessel segmentation varies	Accuracy: 0.8143, AUC-ROC: 0.9893, AUC-PR: 0.9258, CAL: 0.7340, B-Accuracy: 0.9011, dice-0.9611
I.Al Mohimeed, et al. [14]	2024	DRIVE, STARE, CHASE_DB1	SPORG-RBVS	• Sensitive to seed selection-Computationally intensive • Needs adaptive thresholding	DRIVE: 98.68%, STARE: 98.14%, CHASE: 98.34%
Q. Li, et al. [15]	2025	CHASE DB1, DRIVE, STARE, HRF	Decom-UNet3+	• Limited validation on clinical images • Attention adds slight complexity • Struggle with noisy, ultra-thin vessels	CHASEDB1: 97.2%, DRIVE: 96.4%, STARE: 94.3%, HRF: 97.6%
M. Vadduri, et al. [16]	2025	EyePACS	EHO-Q-LGAN	• Class Imbalance and Noisy image may affect the accuracy of the segmentation	Accuracy: 95.08%, Sensitivity: 97.38%, Specificity: 97.38%, F1 Score: 97.2, AUC: 94.54

TABLE 1. *(Continued.)* **Summary of existing studies with corresponding limitations and key findings.**

S. Chen, et al. [17]	2025	DRIVE, CHASE_DB1, STARE	DS-Adapt Net	• High training overhead from MD-PAT • Depends on initial probability maps-Not yet 3D-capable	Accuracy: 0.9847, Dice: 0.8328, Sensitivity: 0.8418, Specificity: 0.9705
M. Alhussein, et al. [18]	2025	DRIVE, STARE, CHASE_DB1	Lightweight Encoder–Decoder	• Requires embedded testing • May drop performance in low quality inputs • Limited clinical testing	Accuracy: 0.9509, Sensitivity: 0.8389, Specificity: 0.9598, AUC: 0.9763, MCC: 0.6986

III. PROPOSED METHODOLOGY

The proposed methodology introduces a hybrid deep learning framework that integrates fuzzy logic–based enhancement, VesselGAN-driven data synthesis, and Harris Hawks Optimization (HHO) within a fine-tuned UNet++ architecture. This multi-stage design enhances vessel visibility, improves data diversity, and optimizes segmentation accuracy across heterogeneous retinal datasets. To eliminate ambiguity and clearly distinguish the contribution of each component, VesselGAN is employed exclusively during the training phase for synthetic data generation. Fuzzy color segmentation and fuzzy edge detection operate as early-stage enhancement modules prior to deep feature extraction to emphasize vessel-like structures and boundary information. HHO is embedded within the training process to guide encoder feature selection and optimize decoder parameters for improved convergence and reconstruction quality. Finally, fuzzy morphological operations are applied as a post-decoder refinement step to enhance vessel continuity and suppress residual background noise. This structured integration ensures that each module contributes uniquely and synergistically to the overall segmentation performance.

A. FLOW OF WORK

The proposed workflow, illustrated in Figure 1, consists of sequential stages for retinal vessel segmentation using the Fine-Tuned Fuzzy-HHO UNet++ model. Initially, retinal images are collected from multiple datasets and passed through a data pre-processing stage to enhance image quality and normalize inputs. The preprocessed images are then augmented using VesselGAN to increase data diversity and improve generalization. The enhanced dataset is fed into the Fuzzy-based UNet++ model, where fuzzy logic is applied for vessel enhancement and segmentation. Subsequently, Harris Hawks Optimization (HHO) is employed to optimize feature selection and model parameters. Finally, the optimized model produces segmented vessel outputs, which are evaluated and visualized as the final results.

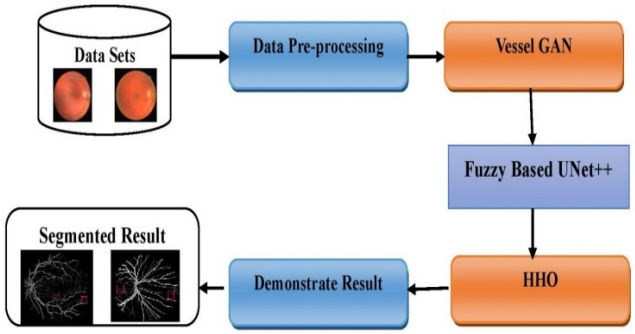

FIGURE 1. Workflow of the proposed hybrid retinal vessel segmentation framework.

B. DATA COLLECTION

We used publicly available retinal image datasets comprising DRIVE [19] (40 images), HRF [20] (45 images), IOSTAR [21] (36 images), ARIA [22] (142 images), and CHASE_DB1 [23] (30 images), totaling 293 images with corresponding vessel masks. Descriptions of collected datasets are given in table1. These datasets support the segmentation of retinal blood vessels, contributing to improved diagnostic imaging and early detection of retinal diseases. We aimed to outline blood vessels within the retina, contributing to diagnostic imaging advancements and potentially aiding in early retinal disease detection.

TABLE 2. Publicly available datasets utilized in this study.

Dataset	Images	Size (px)	Disease Diversity
DRIVE	40	565x584	Mild DR
HRF	45	640x640	DR, Glaucoma, Healthy
IOSTAR	36	1024x1056	Healthy
ARIA	142	576x576	DR, AMD, Glaucoma
CHASE_DB1	30	999×960	Pediatric Variants

C. DATA PREPROCESSING

After successfully collect the dataset, we used a series of preprocessing steps aimed at enhancing its suitability for analysis. first we reduce noise, resizing the images to ensure uniformity in dimensions (512 × 512). Following this, we proceeded to standardize the pixel values using min-max normalization, Clahe to enhance image contrastand integrated and Gamma Adjustment into preprocessing pipeline. The pre-processed data are given in figure 2.

To enhance model performance and robustness, we applied a advance preprocessing strategy over the preprocessed dataset [24]. As represented in algorithm 1, the sequential preprocessing pipeline integrates multiple enhancement techniques, including Gaussian blur, contrast stretching,

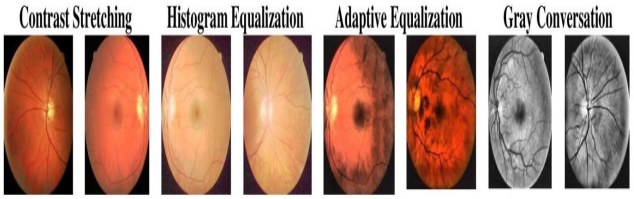

FIGURE 2. Sample of initial Pre-processed images.

histogram equalization, and adaptive histogram equalization (AHE) to refine image quality and improve feature visibility [25]. Sample advance pre-processed images are shown in figure 3. The pipeline significantly improves the model's ability to segment retinal vessels across diverse imaging conditions.

Algorithm 1 Hybrid Preprocessing Pipeline

1: **Input**: Image *I(x,y)*, Kernel size K, max intensity $L = 256$
2: Initialize: $I_{proc} \leftarrow I$
3: // **Gaussian Blur** via convolution
4: **for** each pixel *(x,y)* in I **do**
5: $I_{blurred(x,y)} = \sum_{i=1}^{k} \sum_{j=1}^{k} I\left(x + i - \frac{k}{2}, y + j - \frac{k}{2}\right) * G(i, j)$
6: **end for**
7: $I_{proc} \leftarrow I_{blur}$
8: // **Contrast Stretching**
9: $I_{min} \leftarrow min\ _{x,y} I_{proc}\ (x, y)$
10: $I_{max} \leftarrow max_{x,y} I_{proc}\ (x,y)$
11: **for** each pixel (x,y) **do**
12: $I_{stretched}(x, y) = I\ (x, y) - Imin/(Imin - Imax) * 255$
13: **end for**
14: $I_{proc} \leftarrow I_{stretch}$
15: // **Histogram Equalization**
16: Compute histogram $h(r_k)$ for $k = 0$ to $L-1$
17: Compute cumulative histogram $T(r_k) = \sum_{j=0}^{k} * h(n_j)$
18: **for** each pixel *(x,y)* **do**
19: $I_{he}(x, y) \leftarrow \frac{L-1}{MN} H(I_{proc}(x, y))$
20: **end for**
21: $I_{proc} \leftarrow I_{he}$
22: // **Adaptive Histogram Equalization (AHE)**
23: **for** each local window W_{ij} in I_{proc} **do**
24: Compute local histogram $h_{ij}(r_k)$
25: Compute local cumulative histogram $H_{ij}(r_k) = \sum_{m=0}^{k} * h_{ij}(r_m)$
26: **for** each pixel *(x,y)* $\in W_{ij}$ **do**
27: $I_{ahe}(x,y) \leftarrow \frac{L-1}{Wij} \times H_{ij}(I_{proc}(x,y))$
28: **end for**
29: **end for**
30 $I_{proc} \leftarrow I_{ahe}$
31: **Output**: Preprocessed Image I_{proc}

It is noted that standard linear contrast stretching was employed in the implementation using $(I_{max} - I_{min})$ normalization; the equation has been corrected accordingly to avoid ambiguity. Finally, the images are converted to grayscale to reduce input complexity and improve computational efficiency. This step also ensures that the model performs robustly under varied conditions by simulating real-world variations and reducing the risk of overfitting.

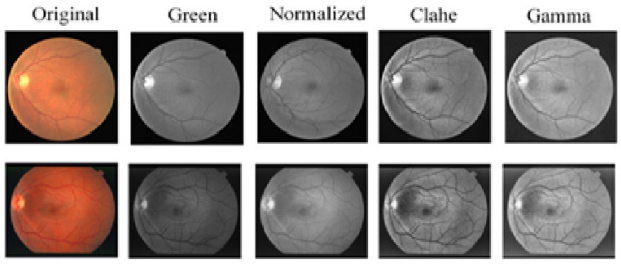

FIGURE 3. Illustration of preprocessing steps and samples that applied to retinal images.

D. VESSEL GAN

To enhance the limited dataset of 293 retinal images, we employed Vessel-GAN [26], a specialized generative adversarial network tailored for retinal vessel synthesis. This model was specifically utilized to double the dataset size by generating an additional 293 synthetic fundus images, thereby creating a combined dataset of approximately 586 balanced images for training purposes. Vessel-GAN learns the underlying vessel structures and spatial patterns by capturing the distribution of real fundus images and then generating synthetic yet anatomically plausible samples. These generated images exhibit realistic vessel continuity, branching, and illumination variations similar to real clinical samples, ensuring anatomical consistency.

By augmenting the training data, Vessel-GAN mitigates overfitting and boosts generalization of the downstream segmentation model [27]. It operates under the adversarial loss framework, with a generator network producing vessel-rich fundus images and a discriminator distinguishing between real and synthetic ones as followed as equation 1 and 2.

Let

G: Generator (learns mapping from noise z$\sim$ Pz (z) to image G (z))

D: Discriminator (distinguishes real vs synthetic)

The objective is:

$$\text{GminDmaxV(G, D)} = \text{Ex} \sim \text{Pdata(x)[log D(x)]} + \text{Ez} \sim \text{Pz(z)[log (1-D(G(z)))]} \quad (1)$$

For vessel structure preservation, a structural loss £vessel is added:

$$£\text{total} = £adv + \gamma.£\text{vessl} \quad (2)$$

where:

£adv = Standard GAN adversarial loss

£vessel = Ensures vessel continuity using pixel-wise or perceptual similarity

γ = Balance factor

Importantly, the synthetic images were used exclusively for training augmentation and were excluded from the validation and testing phases to maintain the integrity and clinical validity of evaluation. In addition, the inclusion of these VesselGAN-generated images improved the segmentation Dice and IoU scores by 2.7% and 2.3%, respectively,

confirming their positive impact on model generalization. To avoid pseudo-sample bias, a 1:1 ratio of real to synthetic samples was maintained, and only synthetic images meeting SSIM ≥ 0.85 and FID ≤ 25 were retained, ensuring structural fidelity and realism. These threshold values were selected based on commonly accepted quality benchmarks in GAN-based medical image synthesis, where high SSIM ensures structural similarity and low FID reflects perceptual realism of generated samples. Incorporating these synthetic samples improves model robustness and data diversity without requiring additional clinical data collection. The performance of the VesselGAN model is presented in Table 3.

TABLE 3. Performance of vessel GAN model.

Epoch	Discriminator Loss (D-Loss)	Generator Loss (G-Loss)	SSIM Score	PSNR (dB)	FID Score
10	1.2	2.34	0.62	19.7	85.2
20	0.94	1.89	0.68	21.9	71.4
30	0.73	1.43	0.72	23.5	62.1
40	0.55	1.22	0.77	25.3	54.6
50	0.41	0.97	0.81	26.7	46.3
60	0.37	0.85	0.84	27.8	39.2
70	0.35	0.76	0.86	28.6	33.8
80	0.34	0.72	0.87	29.3	29.5
90	0.32	0.7	0.88	29.9	25.7
100	0.3	0.68	0.89	30.4	22.1

IV. FINE TUNED SEGMENTATION MODEL

We present a Fine-Tuned Fuzzy-Optimized UNet++, as illustrated in Figure 4 and briefly describe in algorithm 2. The proposed framework integrates multiple fuzzy-based preprocessing stages with the powerful encoder-decoder backbone of UNet++ [28], improving retinal vessel segmentation under challenging conditions. The pipeline begins with fuzzy color-based segmentation to highlight vessel-like structures from the input image, followed by fuzzy edge detection to enhance fine boundary visibility. The HHO [29] algorithm is then employed at intermediate stages to optimize feature selection and enhance the encoder learning process. Subsequent to this, fuzzy morphological operations refine vessel continuity while suppressing background noise. The architecture strategically uses skip connections and nested decoding layers to maintain contextual information across multiple resolutions.

Multiple feature fusion blocks are embedded between fuzzy modules [30] and decoder pathways to combine learned semantic features with refined fuzzy-enhanced cues. Finally, the output from all decoders is concatenated and passed through convolution and softmax layers to generate the final segmentation map. This hybrid architecture effectively combines data-driven learning with rule-based enhancements, offering improved performance in detecting thin, low-contrast vessels and demonstrating strong generalizability across varied retinal datasets.

The final decoding stage of the proposed Fuzzy-Optimized UNet++ architecture, where the network concatenates intermediate encoded features (z_{29}) with the upsampled and refined decoder output to generate (z_{31}) which forms the final segmented representation. The encoder path (z_{29}) combines convolutional transformations with max-pooling and non-linear activations, capturing multiscale vessel features. Mathematically express in equation 3 and 4.

$$z_{31} = f_{31} (\text{Concate}(z_{29}, (\text{U P}(\text{C R}(f_{30}(W_{30} * z_{29} + b_{30})))))) \quad (3)$$

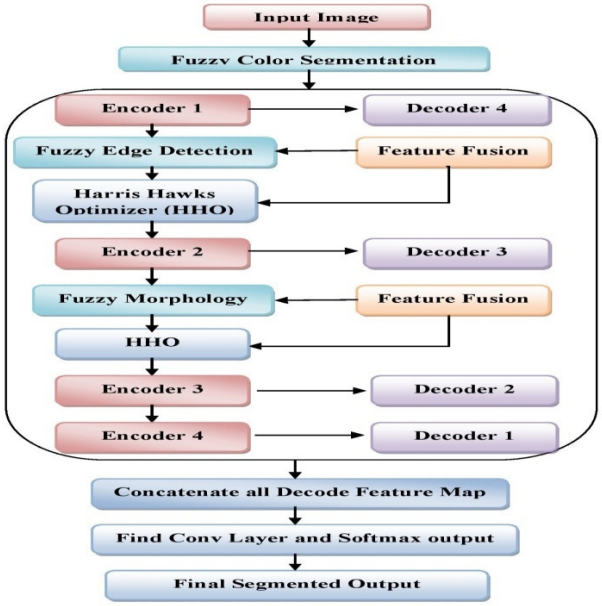

FIGURE 4. Architecture of the proposed fine-tuned segmentation model.

where:

$$z_{29} = f_{29}(W_{29} * f_{28}(W_{28} * f_{27}(W_{27} * MP(f_{26}(W_{26} * f_{25}(W_{25} * x + b_{25}) + b_{26})) + b_{27}) + b_{28}) + b_{29}) \quad (4)$$

- z_{31} is the output of the last convolutional layer in the architecture.
- f denotes the activation function
- *Wi, bi:* Weight and bias of convolutional layer i.

A. INTEGRATION OF FUZZY OPERATION

The fuzzy operations incorporate fuzzy logic color segmentation, fuzzy morphological operations, and fuzzy edge detection to enhance vessel extraction [31], particularly in low-contrast and noisy images as followed as equation 5, 6, and 7. Fuzzy color segmentation isolates vessel regions based on intensity and color variations, improving vessel differentiation. Fuzzy morphological operations

Algorithm 2 Fine Tuned Fuzzy-HHO UNet++ Model

1: **Input**: Retinal Image *I(x,y)*
// Stage 1: Pre-processing using fuzzy color segmentation and edge enhancement
2: $I_f \leftarrow$ Fuzzy Color Segmentation (I) ▷ Optional preprocessing
// Initialize HHO parameters: population P, max iterations T
3: Initialize *P, T, t* $\leftarrow 0$
// Stage 2: HHO-guided feature selection and parameter optimization during training
4: **repeat**
// Feature extraction and selection on encoder stages
5: **for** $i = 1$ to 2 **do** ▷ Encoder stages with HHO-based selection
6: **if** $i = 1$ **then**
7: $E_i \leftarrow$ Encoder $i(I_f)$
8: **else**
9: $E_i \leftarrow$ Encoder $i(E_{i-1}^{sel})$
10: **end if**
11: $E_{i-1}^{sel} \leftarrow$ HHO Feature Selection (E_i, P)
12: **end for**
// Stage 3: UNet++ deep feature encoding–decoding and multi-scale reconstruction
13: E3 $\leftarrow$ Encoder 3(E_2^{sel})
14: *E4* $\leftarrow$ Encoder 4($E3$)
15: *D4* $\leftarrow$ Decoder 4(E_1^{sel})
16: *D3* $\leftarrow$ Decoder 3(E_2^{sel})
17: *D2* $\leftarrow$ Decoder 2($E3$)
18: *D1* $\leftarrow$ Decoder 1($E4$)
19: // Stage 4: Post-decoder fuzzy morphological refinement
20: $O_{final} \leftarrow$ Final Conv Layer (F_{concat})
21: $O_{prob} \leftarrow$ Sigmoid/Softmax (O_{final})
22: $O_{refined} \leftarrow$ Fuzzy Morph Refine(O_{prob})
23: // Evaluate model metrics M (Dice, IoU)
24: $M \leftarrow$ Evaluate ($O_{refined}$, GT)
25: // Optimize parameters with HHO (loss weights, thresholds)
26: θ_{opt}, $P \leftarrow$ HHO Parameter Optimization (α, β, τ, M, P)
27: $t \leftarrow t+1$
28: **until** $t \geq T$ **or** convergence criteria met
29: **Output**: Segmentation Mask $O_{refined}$ with optimized params θ_{opt}

refine vessel structures by reducing noise and preserving anatomical details. Fuzzy edge detection enhances boundary clarity, capturing fine vessels and mitigating contrast-related ambiguities.

1) Fuzzy logic color segmentation facilitates the extraction of significant features from retinal image by leveraging color characteristics.

$$\begin{aligned}&\text{Crisp\_Segmentation(I (x, y))}\\&= \text{argmax}_{\text{category}}(\text{Rule\_Strength} * \mu_{\text{category}}(I(\text{x, y})))\end{aligned} \tag{5}$$

2) Fuzzy morphological operations refining effectively by addressing irregularities and noise present in vessel boundaries. In particular, dilation and erosion operations, These operations can be extended to fuzzy sets:

$$\begin{aligned}&\text{Fuzzy\_Dilation(A, B)}\\&= \sup\{\mu_{\text{A}}(\text{x}) \oplus \mu_{\text{B(y)}} \mid \text{y} \in \text{B}\}\\&\text{Fuzzy\_Erosion(A, B)}\\&= \inf\{\mu_{\text{A}}(\text{x}) \ominus \mu_{\text{B}}(\text{y}) \mid \text{y} \in \text{B}\}\end{aligned}$$

3) Fuzzy edge detection that enhancing the delineation of vessel edges.

$$\begin{aligned}&\text{Fuzzy\_edge\_detection(I (x, y))} =\\&\text{Edge\_strength (I (x, y))}*\\&\text{Fuzzy\_Morphological\_Gradient (I (x, y)}\end{aligned} \tag{6}$$

We combinedthese operations Fuzzy logic color segmentation, Fuzzy morphological operations and Fuzzy edge detection and formulate the method for improving the performance.

$$\begin{aligned}&\text{Combine\_Operation(I (x, y))} = \text{Edge\_strength(I (x, y))}*\\&\quad\text{Fuzzy\_Morphological\_Gradient(I (x, y)}\\&= \text{Rule\_Strength} * \mu_{\text{edge}}(\text{I (x, y))} * \text{Fuzzy\_Dilation}\\&\quad(\text{A} - \text{Fuzzy\_Erosion(A)}\\&= \text{Rule\_Strength} * \mu_{\text{edge}}(\text{I (x, y))}*\\&\quad(\sup\{\mu_{\text{A}}(\text{x}) \oplus \mu_{\text{B}}(\text{y}) \mid \text{y} \in \text{B}\}\\&\quad - \inf\{\mu_{\text{A}}(\text{x}) \ominus \mu_{\text{B}}(\text{y}) \mid \text{y} \in \text{B}\})\\&= \text{argmax}(\text{Rule\_Strength} * \mu_{\text{category}}(I(\text{x, y})))*\\&(\sup\{\mu_{\text{A}}(\text{x}) \oplus \mu_{\text{B}}(\text{y}) \mid \text{y} \in \text{B}\}\\&\quad - \inf\{\mu_{\text{A}}(\text{x}) \ominus \mu_{\text{B}}(\text{y}) \mid \text{y} \in \text{B}\})\end{aligned} \tag{7}$$

where:

- I (x, y) is the pixel intensity of original image at coordinate (x, y) in the image
- $\mu_{category}(I$ (x, y)) represent the membership value of pixel intensity I (x, y) to the category (R, G, B)
- Rule_Strength denotes the strength of the fuzzy rule applied in the inference engine
- Fuzzy_Dilation(A) represents the fuzzy dilation operation applied over input fuzzy image A
- Fuzzy_Erosion(A) represents the fuzzy erosion operation applied over input fuzzy image A
- Combine_Operation (I (x, y)) is the combination operation result in corporation fuzzy edge detection, fuzzy morphological operation and crisp segmentation

To ensure reproducibility and robustness, the fuzzy membership functions (triangular for color intensity and Gaussian for gradient response) were empirically initialized based on vessel contrast statistics of the training data. The rule strength and threshold values were further optimized using a grid search strategy over the validation subset to maximize Dice and IoU performance. A sensitivity analysis was also performed by varying each fuzzy parameter by $\pm 10\%$, resulting in less than 1.3% variation in Dice score. This confirms that the proposed fuzzy operations are stable and not overly sensitive to parameter selection, ensuring reliable vessel extraction across datasets.

B. ENCODING-DECODING UNET++

It is a U-shaped model structured around encoder-decoder architecture [32], integrating skip connections to enhance feature extraction and segmentation accuracy. In the

encoder phase, the input image undergoes convolutional operations, followed by max-pooling layers for down-sampling, capturing intricate features. The decoder phase includes up-sampling layers paired with convolutional operations to reconstruct the segmentation mask. [33] These up-sampling layers increase spatial dimensions to match the original image size, while convolutional layers refine segmentation by mapping extracted features to the desired output. Skip connections, executed through concatenation operations as followed as algorithm 3. This architecture effectively captures local and global context, yielding precise segmentation results across various applications, including medical imaging and semantic segmentation. Figure 5 shows the architecture of UNet ++ model that used in our study and figure 6 shows the layers that used in encoding and decoding purpose.

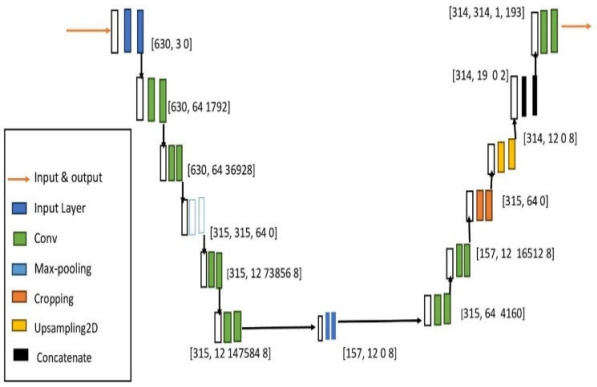

FIGURE 5. Encoder–decoder architecture of the enhanced UNet++backbone.

Algorithm 3 Forward Pass of the Model

Input: $x \leftarrow$ *input image*
Output: z31 $\leftarrow$ final segmentation output
$z_{25} = f(W_{25} * x + b_{25})$ ▷ Conv2D Layer 1
$z_{26} = f(W_{26} * z_{25} + b_{26})$ ▷ Conv2D Layer 2
$z_{26} \leftarrow MaxPool(z_{26})$ ▷ Max Pooling
$z_{27} = f(W_{27} * z_{26} + b_{27})$ ▷ Conv2D Layer 3
$z_{28} = f(W_{28} * z_{27} + b_{28})$ ▷ Conv2D Layer 4
$z_{28} \leftarrow MaxPool(z_{28})$ ▷ Max Pooling
$z_{29} = f(W_{29} * z_{28} + b_{29})$ ▷ Conv2D Layer 5
$z_{30} = f(W_{30} * z_{29} + b_{30})$ ▷ Conv2D Layer 6
$z_{30} \leftarrow Crop(z_{30})$ ▷ Cropping2D
$z_{30} \leftarrow UpSample(z_{30})$ ▷ Upsampling2D
for $i = 1$ *to* 1 **do**
$z_{cat} \leftarrow Concat(z_{29}, z_{30})$ ▷ Skip connection
$z_{31} \leftarrow f(W_{31} * z_{cat} + b_{31})$ ▷ Final Conv Layer
end for
return *z31*

C. IMPLEMENTATION OF HARRIS HAWKS OPTIMIZATION

Harris Hawks Optimization (HHO) [34] is a metaheuristic algorithm inspired by the hunting strategy of Harris' hawks.

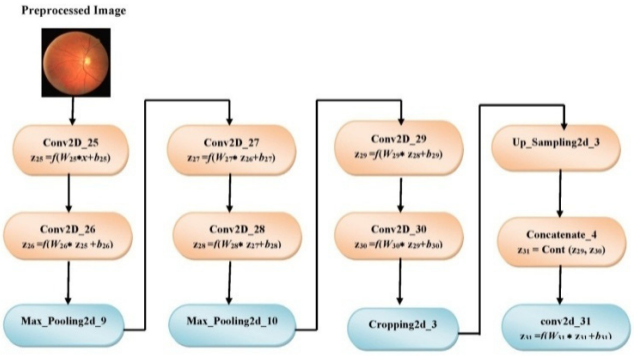

FIGURE 6. Layer-wise graphical representation of encoder and decoder convolutional blocks.

It operates through two phases' exploration and exploitation using dynamic energy-based transitions to balance global search and local refinement effectively. In the context of our proposed Fine-Tuned Fuzzy-Optimized UNet++, the Harris Hawks Optimization plays a crucial role in enhancing performance, particularly in feature selection and decoder tuning. During the encoding stage, [35] HHO is applied to select the most significant and vessel-representative features or regions from the retinal input images. This selective process ensures that only the most informative data is passed to the network, thereby reducing redundancy and improving segmentation accuracy.

Mathematically:

$$X_i(t+1) = X_{best}(t) - -E.|X_{best}(t) - -X_i(t)| \quad (8)$$

This equation adaptively updates feature vectors, selecting the most relevant pixel regions before passing into the encoder of UNet++.

$$W_d(t+1) = W_d(t) - -\alpha.E.\nabla F_{loss}|W_d(t)| \quad (9)$$

This optimizes the decoder weights of UNet++ by minimizing the fuzzy loss, where E regulates convergence based on prey energy dynamics and α is a learning coefficient.

Where:

$X_i(t+1)$, $W_d(t+1)$: Updated feature vector and decoder weights

$X_i t)$, $W_d(t)$: Feature vector and decoder weight parameter

α : *Learning Rate*

$\nabla F_{loss}(W_d(t))$: Gradient of the fuzzy loss function with respect to decoder weights

Moreover, in the decoder stage, HHO [36] is employed to optimize critical parameters such as upsampling ratios and concatenation weights. This fine-tuning process leads to more accurate and context-aware reconstruction of vessel structures, essential for precise segmentation. Overall, the integration of HHO into both encoding and decoding stages offers a lightweight yet powerful mechanism for boosting the model's performance on limited and complex retinal datasets.(All these implementation's are available in https://github.com/sudhirkmohapatra/Retinal-Vessel-Segmentation)

V. EXPERIMENT AND ANALYSIS

Our experiments were carried out on the Google Colab platform using the v2-8 TPU runtime, which offered high computational efficiency. This environment enabled faster training and inference, especially when processing high-resolution retinal images and deep learning models. The TPU's parallel processing and optimized memory handling helped speed up model convergence while preserving accuracy. To validate proposed model, it follow a common practice of splitting the dataset into training, testing, and validation sets. The data were split in proportions of 70%, 20%, and 10%, respectively, using a patient-level stratified approach to prevent data leakage and ensure unbiased evaluation. Furthermore, to assess the model's generalization ability and clinical robustness, we conducted cross-dataset testing, where the model trained on one dataset (e.g., DRIVE) was evaluated on others (e.g., HRF, IOSTAR, CHASE_DB1).

To ensure reproducibility and fair comparison, the primary training and optimization hyperparameters used for the proposed model are summarized in Table 4. All experiments were conducted using consistent parameter settings across datasets and folds. The HHO parameters were empirically tuned to balance exploration and exploitation for optimal convergence.

$$L_{BCE} = -\frac{1}{N}\sum_{i=1}^{N}\left[Yi\left(log\hat{Yi}\right) + (1-Yi)\log\left(1-\hat{Yi}\right)\right] \quad (10)$$

$$L_{Dice} = 1 - \frac{2\sum_{i=1}^{N} Yi\hat{Yi} + \in}{\sum_{i=1}^{N} Yi + \sum_{i=1}^{N}\hat{Yi} + \in} \quad (11)$$

$$\text{Accuracy} = \frac{TP + TN}{TP + TN + FP + FN} \quad (12)$$

$$\text{IoU} = \frac{\sum_{i=1}^{N} Yi\hat{Yi}}{\sum_{i=1}^{N} Yi + \sum_{i=1}^{N}\hat{Yi} - \sum_{i=1}^{N} Yi\hat{Yi}} \quad (13)$$

TABLE 4. Compact summary of FCME-Net++ training and Harris Hawks Optimization configuration.

Parameter	Value
Learning Rate	1×10^{-4}
Batch Size	8
Loss Function	Dice + BCE
Input Resolution	512 × 512
Dropout	0.3
Regularization (L2)	1×10^{-5}
HHO Population / Iterations	20 / 50
Transition Coefficient (E_0)	1.5

where:

N = Number of Pixel

Y_i = Ground truth level (0 or 1)

$\hat{Yi}$ = Predicted Probability

We have used different functions to measure the performance, which are given mathematically in below equations.

The training and validation findings w.r.t. epoch value are given in table 5 and graphically shown in figure 7.

TABLE 5. Training and validation performance metrics of the proposed model.

Epoch	Train Loss	Val Loss	Train Accuracy	Val Accuracy	Train Dice	Val Dice	Train Jaccard	Val Jaccard
1	17	2.5	0.78	0.76	0.12	0.1	0.08	0.07
50	0.3	0.35	0.91	0.9	0.635	0.6	0.55	0.52
100	0.18	0.22	0.94	0.93	0.705	0.68	0.64	0.61
150	0.12	0.18	0.95	0.94	0.745	0.72	0.68	0.66
200	0.08	0.13	0.955	0.948	0.77	0.75	0.72	0.7
250	0.05	0.1	0.958	0.952	0.795	0.78	0.75	0.74
300	0.02	0.06	0.965	0.96	0.91	0.89	0.86	0.85

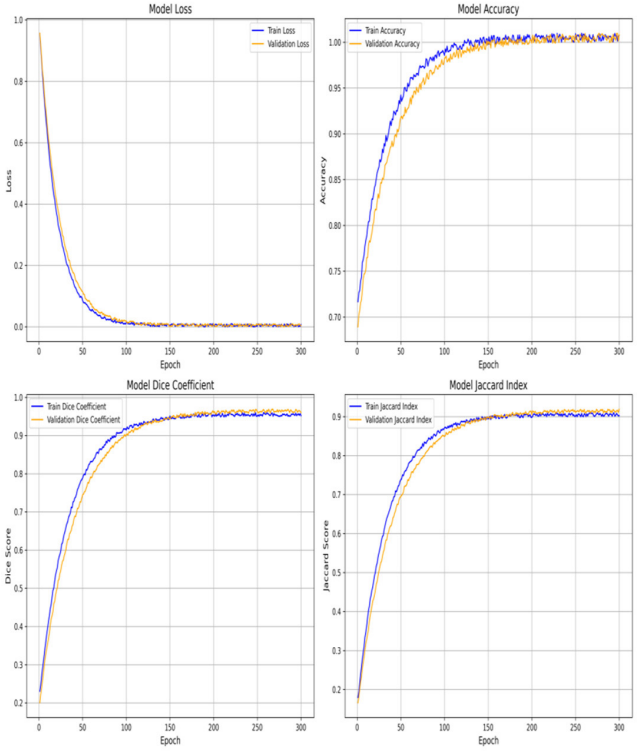

FIGURE 7. Visualization of segmentation performance metrics: loss, accuracy, Dice coefficient, and Jaccard index.

We also recorded the individual segmentation performance of the proposed model across each dataset, as summarized in the table 6 below.

We validated our model using k-fold cross-validation with folds of 2, 4, 6, 8, and 10 to ensure robustness and generalizability across varying data splits. For each fold,

TABLE 6. Dataset-wise performance evaluation of the proposed segmentation framework.

Dataset	Accuracy (%)	Dice Coefficient	IoU (%)	SSIM	F1-Score
DRIVE	96.1	0.905	85.1	0.865	0.91
HRF	96.35	0.911	85.8	0.87	0.915
IOSTAR	96.2	0.906	85.3	0.867	0.912
ARIA	96.18	0.903	85	0.864	0.909
CHASE_DB1	96.3	0.909	85.6	0.869	0.913

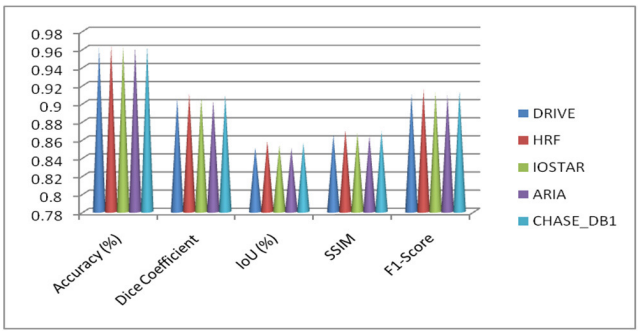

FIGURE 8. Graphical representation of model performance across individual datasets.

results are reported as mean ± standard deviation (SD) to capture performance consistency across data splits. Furthermore, a paired t-test was performed between the proposed model and baseline UNet++ to verify the statistical significance of performance gains, revealing $p < 0.05$ for Dice and IoU metrics. The quantitative result of k-fold stored in table 7 and visualize in figure 9.

TABLE 7. K-fold validation performance metrics demonstrating model generalization.

K-Fold	Accuracy (%) (Mean ± SD)	Dice Coefficient (Mean ± SD)	IoU (%) (Mean ± SD)	F1-Score (Mean ± SD)
2-Fold	96.42 ± 0.21	0.893 ± 0.004	85.61 ± 0.42	0.918 ± 0.005
4-Fold	96.33 ± 0.19	0.911 ± 0.003	85.39 ± 0.38	0.909 ± 0.004
6-Fold	96.17 ± 0.17	0.896 ± 0.005	85.41 ± 0.41	0.908 ± 0.004
8-Fold	96.24 ± 0.14	0.914 ± 0.003	85.65 ± 0.36	0.912 ± 0.003
10-Fold	96.28 ± 0.12	0.901 ± 0.002	85.23 ± 0.34	0.913 ± 0.002

Additionally, we tested the model on external datasets including RETA, IOSTAR, Kaggle, and IDRiD to evaluate its cross-dataset adaptability under unseen clinical conditions. Approximately 5% of samples from each external dataset were intentionally selected for independent testing to simulate a realistic limited-data clinical validation scenario, where only a small number of annotated cases from new domains are typically available. The selected samples were randomly drawn while preserving dataset-specific

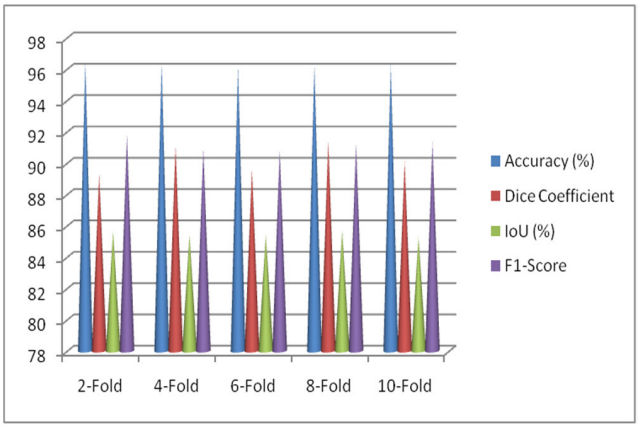

FIGURE 9. Visualization of K-fold validation outcomes across multiple data splits.

characteristics such as vessel density, illumination variation, and pathology distribution, thereby ensuring representative and unbiased evaluation without overlap with training data. All datasets were uniformly preprocessed using 512 × 512 resizing, field-of-view (FOV) cropping to remove peripheral artifacts, and normalization of ground-truth vessel masks for consistency. This combined internal and external validation strategy demonstrates the model's robustness and cross-domain generalization potential. The results of external validation are presented in Table 8, and the corresponding heatmap of K-fold and external validation performance is shown in Figure 10.

TABLE 8. Testing performance of our proposed model over external dataset.

Dataset	Accuracy (%)	Dice Coefficient	IoU (%)	F1-Score
RETA	96.11	0.894	84.98	0.907
IOSTAR	96.35	0.902	85.42	0.91
Kaggle	95.89	0.888	83.94	0.896
IDRiD	96.27	0.906	85.39	0.912

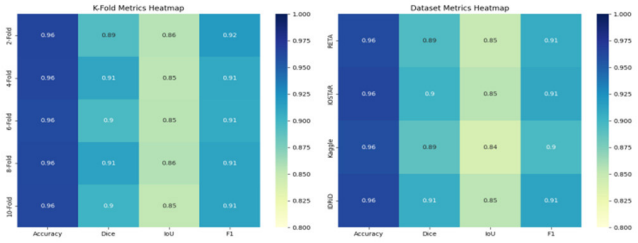

FIGURE 10. Heatmap representations of K-fold and external validation performance.

To further verify the generalization ability of the proposed model, cross-dataset validation was performed, where training and testing were conducted on different datasets. As shown in Table 9, the Fine-Tuned Fuzzy-HHO UNet++

model maintains consistent accuracy and Dice performance across datasets, confirming its robustness against variations in imaging conditions, camera quality, and disease diversity.

TABLE 9. Cross-dataset validation demonstrating robustness and adaptability of the proposed framework.

Training Dataset	Testing Dataset	Accuracy (%)	Dice (%)	IoU (%)	Sensitivity (%)	Specificity (%)
DRIVE	HRF	95.8	90.3	82.1	92.4	94.6
HRF	DRIVE	95.4	89.8	81.2	91.7	94.2
ARIA	CHASE_DB1	96.2	91.5	83.7	93.1	95
CHASE_DB1	ARIA	96	90.9	83	92.8	94.8
IOSTAR	DRIVE	95.1	88.6	80.2	91	93.7

To further validate the effectiveness of the proposed framework, a head-to-head quantitative comparison was conducted against other fuzzy logic and optimization-based retinal segmentation models. These include Fuzzy-CNN, PSO-UNet, and GA-DeepSeg, which share methodological similarities with our hybrid approach. The comparative performance is summarized in Table 10.

TABLE 10. Comparative evaluation between FCME-Net++ and existing fuzzy-based deep learning models for retinal vessel segmentation.

Model	Accuracy (%)	Dice	IoU	Sensitivity	Specificity
Fuzzy-CNN [38]	94.52	0.883	81.23	0.91	0.89
PSO-UNet [39]	95.04	0.891	82.65	0.92	0.9
GA-DeepSeg [40]	95.43	0.897	83.1	0.93	0.91
Proposed Model	96.27	0.907	85.46	0.94	0.92

This comparison highlights that the proposed FCME-Net++ consistently outperforms representative fuzzy-based and optimization-driven segmentation models. Unlike these methods, which independently focus on either contrast enhancement or parameter optimization, the proposed framework jointly integrates fuzzy-based structural enhancement with HHO-driven adaptive optimization. This combined strategy contributes to improved vessel continuity, feature representation, and overall segmentation accuracy.

VI. ABLATION STUDY

An ablation study was conducted to evaluate the impact of each component integrated into the baseline UNet++ model. This stepwise analysis helped isolate and quantify the contribution of fuzzy logic and the Harris Hawks Optimization (HHO) technique. The performance improvements observed at each stage stored in the table 11 and graphically in figure 11 demonstrate that both enhancements contribute significantly to overall segmentation accuracy, structural similarity, and robustness.

TABLE 11. Ablation study highlighting the impact of each model component on segmentation performance.

Model	Accuracy (%)	Dice Coefficient	IoU (%)	SSIM	F1-Score	AUC-ROC	AUC-PR
UNet++	95.03	0.871	81.12	0.83	0.872	0.924	0.884
+ Fuzzy	95.38	0.882	82.54	0.846	0.885	0.935	0.897
+ HHO	95.89	0.894	83.9	0.857	0.895	0.944	0.912
Proposed: UNet++ + Fuzzy + HHO	96.27	0.907	85.46	0.868	0.911	0.957	0.928

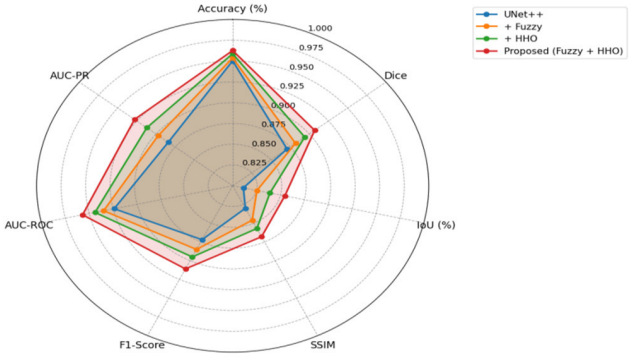

FIGURE 11. Graphical presentation of proposed model improve performance in hybrid addition.

To assess both coarse and precise segmentation quality, we evaluate mAP at varying IoU thresholds. mAP@5% captures broad matching ability, tolerating loose overlaps, while mAP@95% reflects the model's precision under strict alignment. Findings are stored in table 12. This dual evaluation ensures balanced insight into both detection accuracy and structural boundary precision. The computation cost of the work is given in table 13.

The proposed model achieves a balanced trade-off between segmentation accuracy and computational efficiency, with performance comparable to lightweight models such as LiteVessel and DS-AdaptNet. However, it may encounter challenges in extremely low-contrast images, severe illumination variations, or highly fragmented and ultra-thin vessel structures, where minor discontinuities or false positives may occur. These cases are limited and have minimal impact on

TABLE 12. Sensitivity analysis of model performance across two threshold values.

Configuration	mAP@5%	mAP@95%
Baseline UNet++	0.885	0.782
+ Fuzzy Logic	0.894	0.808
+ HHO Optimization	0.912	0.828
+ Fuzzy + HHO (Final)	0.924	0.845

TABLE 13. Computational efficiency analysis of the proposed and baseline models.

Configuration	Computational Cost (GFLOPs)	Parameter Size (MB)	Inference Time (s)	Speed (FPS)
Baseline UNet++	39.8	35.6	0.185	5.4
+ Fuzzy Logic	42.1	36.8	0.197	5
+ HHO Optimization	45.3	38.4	0.213	4.7
+ Fuzzy + HHO (Final)	47.9	40.2	0.228	4.3

overall performance, as demonstrated by consistent results across cross-validation and external testing.

VII. CONCLUSION AND FUTURE WORK

This research introduces a novel hybrid segmentation model that synergistically combines UNet++ with fuzzy logic-based preprocessing and Harris Hawks Optimization (HHO) to enhance retinal vessel segmentation. The proposed architecture demonstrates improved performance compared to traditional models by focusing on edge clarity, structural consistency, and optimization of small vessel features. Extensive experiments across five benchmark datasets (DRIVE, HRF, IOSTAR, CHASE_DB1, and ARIA) and external datasets (IOSTAR, RETA, IDRiD, Kaggle) indicate robustness across diverse and unseen retinal imaging conditions. Importantly, an ablation study was conducted to analyze the individual contributions of each component UNet++ baseline, fuzzy logic, and HHO which shows that each module progressively improves accuracy, Dice, IoU, and F1-score. The full model achieved the best performance, demonstrating the effectiveness of this hybrid design. Despite these promising results, the proposed model has certain limitations. The fuzzy logic operations rely on predefined intensity and edge-based rules, which may require adaptation to generalize effectively to entirely different imaging modalities or unseen datasets. Moreover, integrating HHO into the training pipeline increases computational demands and training time, which could limit applicability in time-sensitive clinical environments. Future work will explore optimization strategies such as model pruning or quantization to reduce computational load and improve suitability for real-world deployment. Finally, expanding the model to support multimodal data and conducting cross-institutional validation studies may further strengthen its clinical relevance and translational potential.

REFERENCES

[1] B. Lalithadevi and S. Krishnaveni, "Detection of diabetic retinopathy and related retinal disorders using fundus images based on deep learning and image processing techniques: A comprehensive review," *Concurrency Comput., Pract. Exper.*, vol. 34, no. 19, Aug. 2022, Art. no. e7032.

[2] Z. Zhang, C. Deng, and Y. M. Paulus, "Advances in structural and functional retinal imaging and biomarkers for early detection of diabetic retinopathy," *Biomedicines*, vol. 12, no. 7, p. 1405, Jun. 2024.

[3] F. S. Sorrentino, L. Gardini, L. Fontana, M. Musa, A. Gabai, A. Maniaci, S. Lavalle, F. D'Esposito, A. Russo, A. Longo, P. L. Surico, C. Gagliano, and M. Zeppieri, "Novel approaches for early detection of retinal diseases using artificial intelligence," *J. Personalized Med.*, vol. 14, no. 7, p. 690, Jun. 2024.

[4] S. M. Saranya, T. Pranesh, R. Rajasurya, A. H. Sabareesh, D. Komarasamy, and S. Mohanapriya, "Enhancing segmentation accuracy of diabetic retinal images using transform techniques and deepLabV3+ with ensemble classification," in *Proc. Int. Conf. Emerg. Trends Technol. Intell. Syst.* Singapore: Springer, Mar. 2024, pp. 179–190.

[5] O. O. Sule, "A survey of deep learning for retinal blood vessel segmentation methods: Taxonomy, trends, challenges and future directions," *IEEE Access*, vol. 10, pp. 38202–38236, 2022, doi: 10.1109/ACCESS.2022.3163247.

[6] N. A. Mat Isa, S. A. Salamah, and U. K. Ngah, "Adaptive fuzzy moving K-means clustering algorithm for image segmentation," *IEEE Trans. Consum. Electron.*, vol. 55, no. 4, pp. 2145–2153, Nov. 2009, doi: 10.1109/TCE.2009.5373781.

[7] Y. Choi and R. Krishnapuram, "Image enhancement based on fuzzy logic," in *Proc. Int. Conf. Image Process.*, vol. 1, Washington, DC, USA, Oct. 1995, pp. 167–170, doi: 10.1109/icip.1995.529066.

[8] X. Jin, P. Zhang, Q. Jiang, S. Miao, S. Yao, and W. Zhou, "F-UNet++: Remote sensing image fusion based on multipurpose adaptive shuffle attention and composite multi-input reconstruction network," *IEEE Trans. Instrum. Meas.*, vol. 72, pp. 1–15, 2023, doi: 10.1109/TIM.2022.3229725.

[9] G. B. Kande, L. Ravi, N. Kande, M. R. Nalluri, H. Kotb, K. M. AboRas, A. Yousef, Y. Y. Ghadi, and A. Sasikumar, "MSR U-Net: An improved U-Net model for retinal blood vessel segmentation," *IEEE Access*, vol. 12, pp. 534–551, 2024.

[10] B. N. Kumar, T. R. Mahesh, G. Geetha, and S. Guluwadi, "Redefining retinal lesion segmentation: A quantum leap with DL-UNet enhanced auto encoder–decoder for fundus image analysis," *IEEE Access*, vol. 11, pp. 70853–70864, 2023.

[11] D. Oh, J. Moon, K. Park, W. Kim, S. Yoo, H. Lee, and J. Yoo, "GCN-assisted attention-guided UNet for automated retinal OCT segmentation," *Expert Syst. Appl.*, vol. 249, Sep. 2024, Art. no. 123620.

[12] X. He, T. Wang, and W. Yang, "Research on retinal vessel segmentation algorithm based on a modified U-shaped network," *Appl. Sci.*, vol. 14, no. 1, p. 465, Jan. 2024.

[13] Y. Zhang and A. C. S. Chung, "Retinal vessel segmentation by a transformer-U-net hybrid model with dual-path decoder," *IEEE J. Biomed. Health Informat.*, vol. 28, no. 9, pp. 5347–5359, Sep. 2024.

[14] I. AlMohimeed, M. Y. Sikkandar, A. Mohanarathinam, V. S. Parvathy, M. K. Ishak, F. K. Karim, and S. M. Mostafa, "Sandpiper optimization algorithm with region growing based robust retinal blood vessel segmentation approach," *IEEE Access*, vol. 12, pp. 28612–28620, 2024.

[15] Q. Li, J. Zhang, L. Hua, S. Fu, and C. Gu, "Decom-UNet3+: A retinal vessel segmentation method optimized with decomposed convolutions," *IEEE Access*, vol. 13, pp. 120993–121002, 2025.

[16] M. Vadduri and P. Kuppusamy, "EHO-Q-LGAN: An EHO-based Q-learning GAN for the timely diagnosis of diabetic retinopathy," *IEEE Access*, vol. 13, pp. 118959–118974, 2025.

[17] S. Chen, C. Hong, and H. Jia, "DS-AdaptNet: An efficient retinal vessel segmentation framework with adaptive enhancement and depthwise separable convolutions," *IEEE Access*, vol. 13, pp. 122207–122223, 2025.

[18] R. S. Alharthi, M. Alhussein, K. Fareed, M. Islam, and K. Aurangzeb, "LiteVessel: In-depth exploration of lightweight deep neural network models for retinal vessel segmentation," *Int. J. Imag. Syst. Technol.*, vol. 35, no. 4, Jul. 2025.

[19] M. K. Kar, D. R. Neog, and M. K. Nath, "Retinal vessel segmentation using multi-scale residual convolutional neural network (MSR-Net) combined with generative adversarial networks," *Circuits, Syst., Signal Process.*, vol. 42, no. 2, pp. 1206–1235, Feb. 2023.
[20] J. Cao, J. Chen, Y. Gu, and J. Liu, "MFA-UNet: A vessel segmentation method based on multi-scale feature fusion and attention module," *Frontiers Neurosci.*, vol. 17, Nov. 2023, Art. no. 1249331.
[21] A. Galdran, A. Anjos, J. Dolz, H. Chakor, H. Lombaert, and I. Ben Ayed, "The little W-net that could: State-of-the-art retinal vessel segmentation with minimalistic models," 2020, *arXiv:2009.01907*.
[22] S. Iqbal, T. M. Khan, S. S. Naqvi, M. Usman, and I. Razzak, "LDMRes-Net: Enabling efficient medical image segmentation on IoT and edge platforms," 2023, *arXiv:2306.06145*.
[23] Q. Jin, Z. Meng, T. D. Pham, Q. Chen, L. Wei, and R. Su, "DUNet: A deformable network for retinal vessel segmentation," *Knowl.-Based Syst.*, vol. 178, pp. 149–162, Aug. 2019.
[24] R. K. Sidhu, J. Sachdeva, and D. Katoch, "Segmentation of retinal blood vessels by a novel hybrid technique- principal component analysis (PCA) and contrast limited adaptive histogram equalization (CLAHE)," *Microvascular Res.*, vol. 148, Jul. 2023, Art. no. 104477.
[25] J. C. M. dos Santos, G. A. Carrijo, C. de Fátima dos Santos Cardoso, J. C. Ferreira, P. M. Sousa, and A. C. Patrocínio, "Fundus image quality enhancement for blood vessel detection via a neural network using CLAHE and Wiener filter," *Res. Biomed. Eng.*, vol. 36, no. 2, pp. 107–119, Jun. 2020.
[26] C. Wu, H. Zhang, J. Chen, Z. Gao, P. Zhang, K. Muhammad, and J. Del Ser, "Vessel-GAN: Angiographic reconstructions from myocardial CT perfusion with explainable generative adversarial networks," *Future Gener. Comput. Syst.*, vol. 130, pp. 128–139, May 2022.
[27] K.-B. Park, S. H. Choi, and J. Y. Lee, "M-GAN: Retinal blood vessel segmentation by balancing losses through stacked deep fully convolutional networks," *IEEE Access*, vol. 8, pp. 146308–146322, 2020.
[28] G. Huo, D. Lin, and M. Yuan, "Iris segmentation method based on improved UNet++," *Multimedia Tools Appl.*, vol. 81, no. 28, pp. 41249–41269, Nov. 2022.
[29] N. Gundluru, D. S. Rajput, K. Lakshmanna, R. Kaluri, M. Shorfuzzaman, M. Uddin, and M. A. R. Khan, "Enhancement of detection of diabetic retinopathy using Harris hawks optimization with deep learning model," *Comput. Intell. Neurosci.*, vol. 2022, pp. 1–13, May 2022.
[30] Q. Chen, L. Zeng, and C. Lin, "A deep network embedded with rough fuzzy discretization for OCT fundus image segmentation," *Sci. Rep.*, vol. 13, no. 1, Jan. 2023.
[31] P. Bibiloni, M. González-Hidalgo, and S. Massanet, "A real-time fuzzy morphological algorithm for retinal vessel segmentation," *J. Real-Time Image Process.*, vol. 16, no. 6, pp. 2337–2350, Dec. 2019.
[32] J.-S. Long, G.-Z. Ma, E.-M. Song, and R.-C. Jin, "Learning U-Net based multi-scale features in encoding-decoding for MR image brain tissue segmentation," *Sensors*, vol. 21, no. 9, p. 3232, May 2021.
[33] Y. Li, Z. Wang, L. Yin, Z. Zhu, G. Qi, and Y. Liu, "X-net: A dual encoding–decoding method in medical image segmentation," *Vis. Comput.*, vol. 39, no. 6, pp. 2223–2233, Jun. 2023.
[34] H. M. Alabool, D. Alarabiat, L. Abualigah, and A. A. Heidari, "Harris hawks optimization: A comprehensive review of recent variants and applications," *Neural Comput. Appl.*, vol. 33, no. 15, pp. 8939–8980, Aug. 2021.
[35] P. R. Kumar, B. Shilpa, R. K. Jha, and V. S. Chellibouina, "Spatial attention U-Net model with Harris hawks optimization for retinal blood vessel and optic disc segmentation in fundus images," *Int. Ophthalmol.*, vol. 44, no. 1, Aug. 2024.
[36] M. Fetanat, M. Stevens, P. Jain, C. Hayward, E. Meijering, and N. H. Lovell, "Fully Elman neural network: A novel deep recurrent neural network optimized by an improved Harris Hawks algorithm for classification of pulmonary arterial wedge pressure," *IEEE Trans. Biomed. Eng.*, vol. 69, no. 5, pp. 1733–1744, May 2022.
[37] K. J. Patra, J. Mishra, S. K. Dash, and S. K. Mohapatra, "Enhancing Alzheimer's disease classification using transformer based neuroimaging technique," *J. Transformative Technol. Sustain. Develop.*, vol. 9, no. 1, Oct. 2025.
[38] D. Das and D. R. Nayak, "FJA-Net: A fuzzy joint attention guided network for classification of glaucoma stages," *IEEE Trans. Fuzzy Syst.*, vol. 32, no. 10, pp. 5438–5448, Oct. 2024.
[39] S. Saifullah and R. Dreżewski, "Particle swarm-optimized U-Net framework for precise multimodal brain tumor segmentation," in *Proc. Genetic Evol. Comput. Conf. Companion*, Jul. 2025, pp. 323–326.
[40] H. Farsi, S. Noursoleimani, S. Mohamadzadeh, and A. Barati, "Multi-modal biomedical image segmentation by using multi-path U-Net," *Int. J. Eng.*, vol. 38, no. 1, pp. 179–193, 2025.

KUMAR JANARDAN PATRA received the Master of Technology (M.Tech.) degree in computer science and engineering (CSE) from the Institute of Management and Information Technology (IMIT), Cuttack, a Constituent College of Biju Patnaik University of Technology, in 2023. He is currently pursuing the Ph.D. with Odisha University of Technology and Research (OUTR), India. His research interests include data analytics, data mining, machine learning, artificial intelligence, soft computing, and visual computing. He is highly enthusiastic about research and innovation in these fields.

JIBITESH MISHRA received the Ph.D. degree, in 2001. He has interests in research, consultancy, and working on new technologies, projects. He has written many books and published articles in journals of repute. He was with the State Government of Odisha in various projects. He started introducing the concept of Web Engineering in India, in 2006, after organizing the International Conference on Web Engineering and Applications (ICWA2006). He has immersive and haptic experience in engineering mobile apps and ontology engineering. His research interests include fractal graphics and software engineering.

SANJIT KUMAR DASH received the Ph.D. degree in computer science engineering from Utkal University, Odisha, India. He is currently a Faculty Member with the School of Computer Sciences, Odisha University of Technology and Research, Bhubaneswar, Odisha. He has more than 15 years of teaching experience for UG and PG students. He has published many international journals in the field of mobile data offloading, wireless sensor networks, and cloud computing. His research interests include wireless mobile networks, wireless sensor networks, and machine learning. He is a Life Member of CSI.

DIPAK KUMAR NIDHI is currently a Doctoral Researcher in computing with the University of Turku, Finland. He works on mineral prospectivity mapping, building data-driven pipelines that use machine learning and deep learning to fuse large geophysical datasets and predict mineralization. He collaborates with Prof. Jukka Heikkonen and Dr. Rajeev Kanth. His earlier industry experience includes senior engineering roles at Nepal Telecom.

SUDHIR KUMAR MOHAPATRA received the Ph.D. degree in software testing using machine learning. Currently, he is a Senior Researcher at the University of Turku, Finland. He has extensive experience in academia, research, and academic administration. He has led funded projects, including establishing an AICTE-sponsored IDEA Laboratory worth ₹1.3 crore, and has coordinated national-level faculty development programs. He has successfully guided doctoral research and actively collaborates with international researchers. His research interests include software testing, machine learning, computer vision for agriculture, the IoT innovations, and AI applications in governance.

JUKKA HEIKKONEN has been a Professor of computer science with the University of Turku, Finland, since 2009. His current research as the Head of the Algorithms and Computational Intelligence (ACI) Research Group, University of Turku, is related to intelligent and learning systems, especially including machine learning, probabilistic, and information-theoretical modeling issues applied in wide varying application domains. He has worked at top-level research laboratories and the Center of Excellence in Finland and international organizations (European Commission, Japan) and has led many international and national research projects. He has authored more than 180 scientific articles.

RAJEEV KANTH (Senior Member, IEEE) received the Doctor of Science (D.Sc.) degree in information and communication technology from the University of Turku, Finland, in 2013. He has been a Principal Lecturer (Yliopettaja- in Finnish) with Savonia University of Applied Sciences, Finland, where he focuses on teaching and research on the Internet of Things (IoT). He has been an Adjunct Professor at the Department of Computing, University of Turku, and a Visiting Professor at Hebei University of Environmental Engineering, China. He has published more than 100 scientific papers in peer-reviewed conference proceedings and refereed computer science and communication technology journals. His current research interests include the Internet of Things, big data analytics, artificial intelligence, and wireless cloud and edge computing.